Ground Penetrating Radar Fourier Pre-processing for Deep Learning Tunnel Defects' Automated Classification

Ground Penetrating Radar Fourier pre-processing for deep learning tunnel defects automated classification

Giulia Marasco[1 [0000−0002−5264−8947]], Marco M. Rosso[1 [0000−0002−9098−4132]], Salvatore Aiello[1 [0000−0002−7101−2637]], Angelo Aloisio[2 [0000−0002−6190−0139]], Giansalvo Cirrincione[3 [0000−0002−2894−4164]], Chiaia Bernardino[1 [0000−0002−5469−2271]], and Giuseppe C. Marano[1 [0000−0001−8472−2956]]

[1] Politecnico di Torino, DISEG, Dipartimento di Ingegneria Strutturale, Edile e Geotecnica, Corso Duca Degli Abruzzi, 24, Turin 10128, Italy, Email: marasco.giulia@polito.it, marco.rosso@polito.it, salvatore.aiello@polito.it, bernardino.chiaia@polito.it, giuseppe.marano@polito.it

[2] Università degli Studi dell'Aquila, via Giovanni Gronchi n.18, 67100 L'Aquila Email: angelo.aloisio1@univaq.it

[3] University of Picardie Jules Verne, Lab. LTI, Amiens, France, exin@u-picardie.fr

Abstract. Nowadays, drawing up plans to control and manage infrastructure assets has become one of the most important challenges in most developed countries. The latter must cope with issues relating to the aging of their infrastructures, which are getting towards the end of their useful life. This study proposes an automatic approach for tunnel defects classification. Starting with non-destructive investigations using Ground Penetrating Radar (GPR), the deep convolutional neural networks (CNN), with and without the application of 2D FT, have allowed the classification of several structural defects (e.g., crack, voids, anomaly, etc.) with high accuracy. The proposed methodology eliminates the need for human interpretation of Ground Penetrating Radar profiles and the use of integrative investigations (e.g., video-endoscopy, core drilling, jacking, and pull-out testing) for defects classification. As a result, it has significant speed and reliability that make it both time and cost-efficient.

Keywords: Road tunnels · Fourier transform · Convolutional Neural Network · Structural Health Monitoring · Ground Penetrating Radar.

1 Introduction

The development of automated systems for monitoring infrastructure current structural state is critical for the implementation of cost-effective maintenance plans that ensure a high level of safety [1,2,3,4,5,6,7]. The extent of the infrastructure heritage in developed countries that

need to be controlled is significant. As a result, developing robust, reliable, and timely structural health monitoring (SHM) programs are especially important for high-impact structures, like bridges [8] and underground structures [9]. Focusing on tunnels, the number of them in the proximity of their design life end, and so at high risk, is extremely high. Degradation phenomena and structural damages may have irreversibly changed the original structural characteristics and severe consequences may occur [10]. As a result, systems that rely exclusively on traditional routine inspections are not sufficient and ineffective [11]. Since they are based on human judgment and require specialist personnel who are frequently exposed to dangerous environments, they are time-consuming and expensive [12]. Image recognition-based structural health monitoring (SHM) algorithms are frequently leveraged to detect the presence and nature of potential infrastructure deterioration [13]. The use of deep convolutional neural networks (CNN) that exploit transfer learning processes has proven effective in many applications [14]. It's really interesting how much support they can provide in identifying and classifying defects that can be extracted from the results of non-destructive structural testing (NDT) techniques. Among the most relevant non-destructive methods, for the quantity and quality of information that can be obtained, emerges the Ground Penetrating Radar (GPR). It overcomes the limitations of visual inspections techniques that are only adapted to detect surface defects [15]. Nevertheless, because GPR data is typically scaled and manually interpreted or stored and subsequently processed off-line, the GPR data analysis is generally computationally costly [16]. This paper presents the results of a proposed multi-level methodology for defect classification starting based on GPR profiles, with and without the use of the 2D Fourier Transform as a pre-processing operation. The obtained outcomes are promising and encourage further developments.

2 Monitoring road tunnels with Ground Penetrating Radar (GRP)

Among the several non-destructive testing (NDT) methods [17] for defect characterization in engineering materials, the Ground Penetrating Radar has been chosen [18]. Due to the ease of use and transportation [19] and to its penetration capacity, such an instrument turned out to be a valuable tool for damage detection, localization, and classification. GPR is a geophysical technique [20] that involves transmitting high-frequency electromagnetic wave impulses into the investigated material using an antenna with a frequency of 10 to 2600 MHz. The propagation of such an impulse is influenced by the dielectric characteristics of the material. The GPR campaign has been focalized on Italian tunnels dated between 1960s and 1980s. Two types of GPR have been used in such campaign. The first uses a dual-frequency antenna, the second involves a high-frequency one. The technical characteristics are shown in the following Tables 1 and 2. GPR profiles have a vertical axis that shows the depth of the examined thickness and a horizontal axis that indicates the progressive distance from the structure's beginning. In the investigation campaign, each Ground Penetrating Radar profile was interpreted by specialized personnel. An example of a GPR profile with defect interpretation is shown in the following Figure 1.

Table 1. Technical characteristics of GPR with dual frequency antenna.

GPR with dual frequency antenna features	value
minimum number of channels	4
pulse repetition frequency (kHz)	400
range (nsec)	0-9999
min. number of scans/second	400
power (Volt)	12
primary dual-frequency antenna (MHz)	400-900
secondary dual-frequency antenna (MHz)	200-600

Table 2. Technical characteristics of GPR with high-frequency antenna.

GPR high-frequency antenna features	value
minimum number of channels	4
pulse repetition frequency (kHz)	400
range (nsec)	0-9999
min. number of scans/second	400
power (Volt)	12
high-frequency antenna (GHz)	≥2

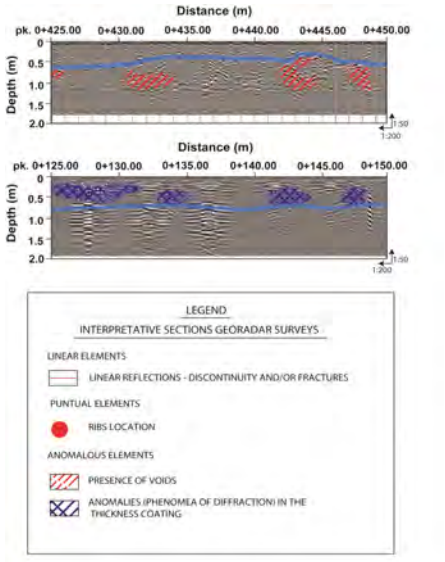

Fig. 1. An example of a GPR profile with defect patterns interpretation by human experts.

3 Two dimensional Fourier Transform for image processing

The Fourier transform (FT) is one of the most powerful tools for signal processing which provides a decomposition of a signal into its fundamental components. Moreover, it performs a domain mapping by changing the representation of the problem by passing from the input (spatial or time) domain to the Fourier or frequency domain. For continuous phenomena, the FT expresses a signal as an infinite sum of harmonics characterized by different frequencies and denoting the frequency content of each one. In real-world, even with the most sophisticated instrumentation, data are collected discretely through a sampling process. The sampling or Nyquist-Shannon theorem states that any continuous signal can be uniquely reconstructed in a reliable way starting from its samples when the sampling frequency is two times the Nyquist frequency, which represents the highest signal representable frequency [21]. Thus, for discrete signals, the Discrete version of the FT (DFT) has been developed to deal with real-world sampled signals.

In general, a digital image is represented by a matrix/tensor of pixels, where each pixel contains certain values. An 8-bit precision gray-scale images is a matrix in which each pixel can assume an integer value between 0 and 255. Whereas, with a red-green-blue (RGB) image, the data are represented by a tensor with a depth-size of three, in which each pixel is represented by three bytes in total because each color channel can assume integer values between 0 to 255 [22]. Without loss of generality, an image can be interpreted as two-dimensional signals of pixel values by looking to vertical and horizontal directions [23]. Therefore, the FT can be adopted to decompose a 2D discrete-space signal (digital image) into its main sinusoidal components. Due to the sampling frequency, only a certain number of harmonics is obtained, enough to fully describe the information contained in the image [24]. Considering a digital image in the spatial domain A of size $n \times m$ with components a_{rs}, with $0 \leq r \leq n-1$, $0 \leq s \leq m-1$, the discrete 2D-FT (2D-DFT) is a matrix F in the Fourier domain of size $n \times m$ with components [22]:

$$f(k,l) = \sum_{r=0}^{n-1} \sum_{s=0}^{m-1} a(r,s) e^{-2\pi i \left(\frac{kr}{m} + \frac{ls}{n}\right)} \tag{1}$$

where $0 \leq k \leq n-1$, $0 \leq l \leq m-1$. The 2D-FT, in practice, performs a sum of the products of the spatial image input with the sinusoidal basis functions, expressed in complex exponential form. The term $f(0,0)$ denotes the direct current (DC) component which is the average brightness of the input image, whereas the last realization $f(n-1, m-1)$ corresponds to the highest frequency component [24]. The inverse 2D-FT (2D-IDFT) is defined as:

$$a(r,s) = \frac{1}{n \cdot m} \sum_{k=0}^{n-1} \sum_{l=0}^{m-1} f(k,l) e^{2\pi i \left(\frac{kr}{m} + \frac{ls}{n}\right)} \tag{2}$$

To lower the computational effort, it is possible to demonstrate that the 2D-DFT can be computed as a series of $2n$ one-dimensional FT [24], which leads to a computational complexity

of $O(n^2)$. Fast Fourier formulations (2D-FFT) have been developed in order to further reduce the complexity to $O(n \log_2(n))$ [24]. The FT operation delivers a complex matrix which can be displayed in terms of real and imaginary parts, or, usually, in terms of magnitude and phase. Since most of the information are contained into the magnitude, the phase is not considered in many applications. However, if it would be necessary to reconstruct again the original image with the 2D-IDFT, the phase information is strictly required in order to avoid corrupted image reconstruction [24]. Since the magnitude may present very scattered values comparing the largest DC component with respect to the other frequencies, a logarithmic transformation is usually applied to enhance the information contained in low-frequency components:

$$\tilde{f}(k,l) = c \log\left(1 + \left|M_{k,l}\right|\right) \tag{3}$$

where c is a scaling factor set to unity in the present study, and

$$M_{k,l} = \sqrt{\mathrm{Re}(f(k,l))^2 + \mathrm{Im}(f(k,l))^2} \tag{4}$$

is the magnitude for each pixel in the frequency domain. Among the many useful properties of the FT, the most important in the present case is related to the convolution property: the convolution operation in the input domain becomes a simple multiplication in the Fourier domain. In image processing, digital filters can be used to smooth the image, by suppressing high frequencies in the image, or to detect edges by removing the low frequencies [24]. These operations are accomplished by a filter kernel function $h(r,s)$ which slides on the image and compute a correlation between the kernel receptive field and the input image: $g(r,s) = h(r,s) * a(r,s)$. Specifically, the convolution is a correlation operation acting with a flipped kernel $h(-r,-s)$. Throughout the convolution property, the above-mentioned computation, which is the core of the convolutional neural networks (CNN), can be performed more efficiently in the frequency domain.

In the present work, the 2D-FFT has been adopted to perform a pre-processing of the road tunnel GPR linings profiles. This may help to compress data, maintaining the geometric structure of the starting digital image. The 2D-FFT identifies the vertical and horizontal patterns in the input image, preserving information of such alignments in the most dominant frequency components in the Fourier domain. Furthermore, as evidenced in the Figure 1, the 2D-FFT allows removing such horizontal periodic components, typical of the GPR profiles in the depth direction. In Figure 2, two illustrative examples have been depicted to highlight the effects of the 2D-FFT pre-processing on the road tunnels GPR profiles.

4 Methodology

The dataset considered in the current study comes from tunnel lining defects classification concerned structures dating from 1960s to 1990s. Specifically, after the human defect recognition, the entire GPR profiles were cut with a constant step of 5.00 m long along the horizontal

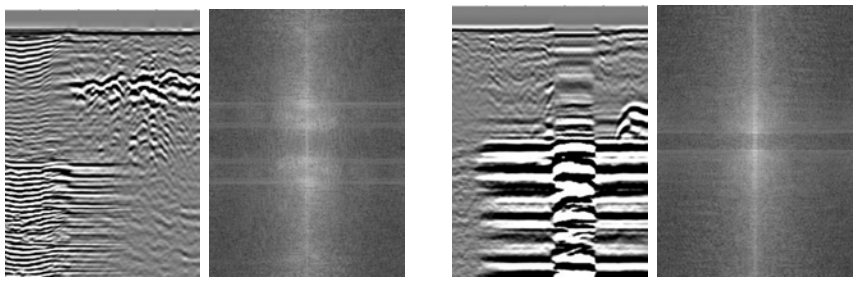

Fig. 2. Two examples of 2D-FFT pre-processing of road tunnels GPR profiles. (a) and (c): samples extracted from the entire GPR profile; (b) and (d): 2D-FFT magnitude pre-processed images.

axis. In this way, sample images were obtained for classification task. These samples have been labeled according to the human experts defect-recognition phase. To avoid that some defects were placed across two different images, the cutting step was occasionally manually altered to provide samples which allowed for a more clear classification.

4.1 Multi-level defect classification

The classification has been performed in a hierarchical multi-level procedure. As depicted in Figure 3, this procedure allowed to perform a more precise classification of the defect. Based on the structure of the hierarchical classification tree, 7 models were trained. Each of them performs a binary classification task. Following in depth the tree depicted in Figure 3, the total number of available samples for each level gradually decrease. Moreover, since each class presents an unbalanced number of images, in order to train a good classification model, a balanced approach was forced by the class with the minimum number of samples. To accomplish the classification tasks, a deep learning model has been trained based on convolutional neural networks, discussed in the following section.

4.2 Convolutional Neural Network: ResNet50

Convolutional neural networks (CNN) algorithms are one of the most used deep learning techniques capable of solving categorization problems based on image recognition. To solve this kind of task, ResNet-50 was trained to detect structural states of tunnels lining through the transfer learning approach. Indeed, such networks are pre-trained on the ImageNet Large Scale Visual Recognition Challenge (ILSVRC) dataset based on 1281167 training, 50000

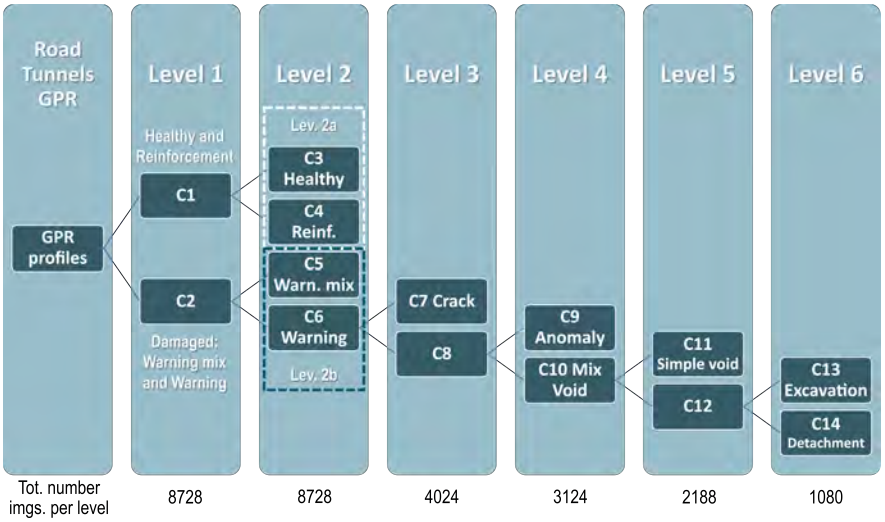

Fig. 3. Hierarchical tree multi-level classification representation.

validation, and 100000 test images [25,26]. The chosen CNN was used within the MATLAB2020b programming environment. Its architecture is composed of 177 layers of which 49 are convolutional and 1 is fully connected and it is designed in 2015 by He K et al [27]. It is defined as a "feed-forward" neural network with "residual/skip connections" that leverages Rectified Linear Units (ReLu) and softmax as activation functions exploiting 25 million parameters. Among the different layers of the network, it is possible to acknowledge the four types of layers that distinguish the neural networks as the activation and pooling layer in addition to those convolutional and fully connected previously cited [28]. The convolutional layer contains neurons that interact with the other one in the next layer through convolutional kernels while the nonlinear features are extracted using the activation layer. The pooling one can reduce the convolutional feature to improve the performance of the algorithm decreasing the cost. The last one is the layer that interprets the extracted features and creates a vector containing the membership probability of each class [29]. In the literature, deeper neural networks are expected to perform better than shallower ones especially in the training phase, as shown in several studies [30,31]. However, it is recognized that the increase in accuracy is not always related to an increase in network depth, which could generate degradation problems. The innovative element that makes ResNet compared to other CNNs is the presence of skip connections (residual units). This particular unit allows the learning of the differences between the input and output layers mitigating, in this way, the problems deriving from the excessive depth. The choice has fallen on ResNet for the depth of the network and for the relatively reduced computational level. In particular, ResNet-50 has been adopted as a

Table 3. ResNet50 hyperparameters set.

Parameter	Value
Learning rate	0.001
Mini-batch size	32
Max epoch	12

pre-trained network to perform a binary classification of GPR profile image and their FFT transform, previously described, using the following hyperparameters, as illustrated in Table 3.

5 Results and Discussion

The classification of tunnel lining defects concerned structures dating from 1960s to 1990s following the procedure described in the previous sections. The results obtained by training the network with the GPR profiles, obtained during the different investigation campaigns, were compared with the results obtained by training the same network with the FTs of the same profiles. Whereas the accuracy obtained following the first approach showed values greater than 90% and with an average of 98.8% [29], the results obtained with the trained ResNet-50 on FTs show values greater than 80% unless level 2b and with an average of 94.4%. Tables from 4 to 10 show the confusion matrices for each level obtained with the FT.

5.1 Confusion matrix for each level

Out of several useful methods for defining the performance of a classifier algorithm, the most well-known is the confusion matrix. For each level of detail, the confusion matrix is reported followed by the accuracy value. The mentioned matrices are composed of rows showing the actual classes and columns representing the predicted labels. The accuracy value is determined by the ratio between the matrix trace and the total sum of its terms. The value of accuracy and the confusion matrix are presented for each level. They are relative to an arithmetic mean of the results obtained through the application of the K-fold validation technique. Besides, for each test fold, an error estimation through the RMSE (Root Mean Square Error) index was performed and then their average was calculated and used as a final indicator. The data for each classification were casually divided into k groups (folds) in which a "fold" is used for testing, one for validation, and (k-2) for network training [32,33]. The used value of k is equal to 10. The choice of this value is based on empirical demonstrations that highlight the ability of it to produce test error rate estimates that have neither excessive bias nor much variance [34].

Table 4. Confusion Matrix – Level 1.

Real Class	C1: predicted	C2: predicted	Performance Metrics
C1	87.9%	12.1%	Accuracy: 88%
C2	11.4%	88.6%	RMSE: 31.5%

Table 5. Confusion Matrix – Level 2a.

Real Class	C3: predicted	C4: predicted	Performance Metrics
C3	79.3%	20.7%	Accuracy: 83.1%
C4	13.0%	87.0%	RMSE: 37.2%

Table 6. Confusion Matrix – Level 2b.

Real Class	C5: predicted	C6: predicted	Performance Metrics
C5	73.5%	26.5%	Accuracy: 76.3%
C6	20.9%	79.1%	RMSE: 44.3%

Table 7. Confusion Matrix – Level 3.

Real Class	C7: predicted	C8: predicted	Performance Metrics
C7	97.8%	0.22%	Accuracy: 94.4%
C8	9.0%	91.0%	RMSE: 20.6%

Table 8. Confusion Matrix – Level 4.

Real Class	C9: predicted	C10: predicted	Performance Metrics
C9	83.9%	16.1%	Accuracy: 85.1%
C10	13.6%	86.4%	RMSE: 38.3%

Table 9. Confusion Matrix – Level 5.

Real Class	C11: predicted	C12: predicted	Performance Metrics
C11	85.7%	14.3%	Accuracy: 90%
C12	5.9%	94.1%	RMSE: 28.6%

Table 10. Confusion Matrix – Level 6.

Real Class	C13: predicted	C14: predicted	Performance Metrics
C13	92.4%	7.6%	Accuracy: 91%
C14	11.3%	88.7%	RMSE: 25.8%

5.2 Comparison with the previous work [29]

The strategy proposed in this work is related to the possibility of using as input data of a CNN, not only GPR profile images, but also the FTs of the same ones. The outcomes obtained with this last one showed a decrease in accuracy for levels 1, 2a, 2b and 4 (keeping an accuracy higher than 90% for the remaining levels) with respect to the results obtained by training ResNet-50 with GPR profiles [29]. Comparing the results of the two different training and test valuation of the ResNet-50 proposed, level 1 (healthy and reinforced/damaged) shows an accuracy of 88% compared to 92.6% previously obtained, level 2a (healthy/reinforced) shows an accuracy of 83.1% compared to 97.3%. The accuracy for level 2b (warning mix/warning) shows a value of 76.3% compared to the respective value of 90.4%. Regarding the accuracy in level 3 (crack/C8) the value obtained by training on the FTs of the GPR profiles equal to 94.4% is very similar to the previous one equal to 95.9%. Level 4 (Anomaly/mix void) shows an accuracy of 85.1%compared to 91.8%. In the last two levels, the CNN with FTs showed the highest accuracy values of 90% and 91% for levels 5 and 6 respectively, compared to the values of 98.2% and 95.3% of the same CNN trained with simple GPR profiles.

6 Conclusions

In the present work, a hierarchical multi-level classification approach is discussed related to road tunnels linings GPR tests for automated defects classification. The GPR profiles are sampled and pre-processed with 2D-FFT technique performing data compression and making convolution more efficient. Seven different CNN models have been trained with the transfer learning approach starting from pre-trained ResNet-50 model. A final comparison with respect to the model trained without image pre-processing pointed out the reliability of the proposed approach for automated road tunnel defects classification. However, the pre-processing phase probably produces an excessive compression of the data, providing lower accuracy levels with respect to the model trained on raw GPR images samples. Future developments of the present work may virtually involve some further comparisons not only from the pre-processing side, but even on the neural architecture which could lead to further improvements and a more reliable system for automated road tunnels linings defect classification.

References

1. Chiaia, B., Marasco, G., Ventura, G., Zannini Quirini, C.: Customised active monitoring system for structural control and maintenance optimisation. Journal of Civil Structural Health Monitoring 10(2), 267–282 (2020)
2. Aloisio, A., Pasca, D.P., Battista, L., Rosso, M.M., Cucuzza, R., Marano, G., Alaggio, R.: Indirect assessment of concrete resistance from fe model updating and young's modulus estimation of a multi-span psc viaduct: Experimental tests and validation. Elsevier Structures 37, 686–697 (01 2022)

3. Rosso, M.M., Cucuzza, R., Aloisio, A., Marano, G.C.: Enhanced multi-strategy particle swarm optimization for constrained problems with an evolutionary-strategies-based unfeasible local search operator. Applied Sciences 12(5) (2022)
4. Asso, R., Cucuzza, R., Rosso, M.M., Masera, D., Marano, G.C.: Bridges monitoring: an application of ai with gaussian processes. In: 14th International Conference on Evolutionary and Deterministic Methods for Design, Optimization and Control. Institute of Structural Analysis and Antiseismic Research National Technical University of Athens (2021)
5. Rosso, M.M., Cucuzza, R., Di Trapani, F., Marano, G.C.: Nonpenalty machine learning constraint handling using pso-svm for structural optimization. Advances in Civil Engineering 2021 (2021)
6. Cucuzza, R., Costi, C., Rosso, M.M., Domaneschi, M., Marano, G., Masera, D.: Optimal strengthening by steel truss arches in prestressed girder bridges. Proceedings of the Institution of Civil Engineers - Bridge Engineering pp. 1–51 (01 2022)
7. Marasco, G., Chiaia, B., Ventura, G.: Ai based bridge health assessment. 9th International Workshop on Reliable Engineering Computing (REC2021) is "Risk and Uncertainty in Engineering Computations" (2021), http://ww2new.unime.it/REC2021/papers/REC2021-39.pdf
8. Chiaia, B., Ventura, G., Quirini, C.Z., Marasco, G.: Bridge active monitoring for maintenance and structural safety. In: International Conference on Arch Bridges. pp. 866–873. Springer (2019)
9. Bhalla, S., Yang, Y., Zhao, J., Soh, C.: Structural health monitoring of underground facilities – technological issues and challenges. Tunnelling and Underground Space Technology 20(5), 487–500 (2005)
10. Di Trapani, F., Tomaselli, G., Sberna, A.P., Rosso, M.M., Marano, G.C., Cavaleri, L., Bertagnoli, G.: Dynamic response of infilled frames subject to accidental column losses. In: Pellegrino, C., Faleschini, F., Zanini, M.A., Matos, J.C., Casas, J.R., Strauss, A. (eds.) Proceedings of the 1st Conference of the European Association on Quality Control of Bridges and Structures. pp. 1100–1107. Springer International Publishing, Cham (2022)
11. Jiang, Y., Zhang, X., Taniguchi, T.: Quantitative condition inspection and assessment of tunnel lining. Automation in Construction 102, 258–269 (2019)
12. Attard, L., Debono, C.J., Valentino, G., Di Castro, M.: Tunnel inspection using photogrammetric techniques and image processing: A review. ISPRS Journal of Photogrammetry and Remote Sensing 144, 180–188 (2018)
13. Lei, M., Liu, L., Shi, C., Tan, Y., Lin, Y., Wang, W.: A novel tunnel-lining crack recognition system based on digital image technology. Tunnelling and Underground Space Technology 108, 103724 (2021)
14. Feng, C., Zhang, H., Wang, S., Li, Y., Wang, H., Yan, F.: Structural damage detection using deep convolutional neural network and transfer learning. KSCE Journal of Civil Engineering 23(10), 4493–4502 (2019)
15. Dawood, T., Zhu, Z., Zayed, T.: Deterioration mapping in subway infrastructure using sensory data of gpr. Tunnelling and Underground Space Technology 103, 103487 (2020)
16. Al-Nuaimy, W., Huang, Y., Nakhkash, M., Fang, M., Nguyen, V., Eriksen, A.: Automatic detection of buried utilities and solid objects with gpr using neural networks and pattern recognition. Journal of Applied Geophysics 43(2), 157–165 (2000)
17. Dwivedi, S.K., Vishwakarma, M., Soni, P.: Advances and researches on non destructive testing: A review. Materials Today: Proceedings 5(2, Part 1), 3690–3698 (2018), 7th International Conference of Materials Processing and Characterization, March 17-19, 2017

18. Tosti, F., Ferrante, C.: Using ground penetrating radar methods to investigate reinforced concrete structures. Surveys in Geophysics 41(3), 485–530 (2020)
19. Davis, A.G., Lim, M.K., Petersen, C.G.: Rapid and economical evaluation of concrete tunnel linings with impulse response and impulse radar non-destructive methods. NDT & E International 38(3), 181–186 (2005), structural Faults and Repair
20. Cardarelli, E., Marrone, C., Orlando, L.: Evaluation of tunnel stability using integrated geophysical methods. Journal of Applied Geophysics 52(2), 93–102 (2003)
21. Farrar, C.R., Worden, K.: Structural health monitoring: a machine learning perspective. John Wiley & Sons (2012)
22. Broughton, S.A., Bryan, K.: Discrete Fourier analysis and wavelets: applications to signal and image processing. John Wiley & Sons (2018)
23. Lim, J.S.: Two-dimensional signal and image processing. Englewood Cliffs (1990)
24. Fisher, R., Perkins, S., Walker, A., Wolfart, E.: Hypermedia image processing reference. England: John Wiley & Sons Ltd pp. 118–130 (1996)
25. Russakovsky, O., Deng, J., Su, H., Krause, J., Satheesh, S., Ma, S., Huang, Z., Karpathy, A., Khosla, A., Bernstein, M., et al.: Imagenet large scale visual recognition challenge. International journal of computer vision 115(3), 211–252 (2015)
26. Markoff, J.: For web images, creating new technology to seek and find. New York Times (2012)
27. He, K., Zhang, X., Ren, S., Sun, J.: Deep residual learning for image recognition. In: 2016 IEEE Conference on Computer Vision and Pattern Recognition (CVPR). pp. 770–778 (2016)
28. Rawat, W., Wang, Z.: Deep Convolutional Neural Networks for Image Classification: A Comprehensive Review. Neural Computation 29(9), 2352–2449 (09 2017)
29. Chiaia, B., Marasco, G., Aiello, S.: Deep convolutional neural network for multi-level non-invasive tunnel lining assessment. Frontiers Of Structural And Civil Engineering (2022)
30. Anitescu, C., Atroshchenko, E., Alajlan, N., Rabczuk, T.: Artificial neural network methods for the solution of second order boundary value problems. Computers, Materials & Continua 59(1), 345–359 (2019)
31. Guo, H., Zhuang, X., Rabczuk, T.: A deep collocation method for the bending analysis of kirchhoff plate. Computers, Materials & Continua 59(2), 433–456 (2019)
32. Rodriguez, J.D., Perez, A., Lozano, J.A.: Sensitivity analysis of k-fold cross validation in prediction error estimation. IEEE Transactions on Pattern Analysis and Machine Intelligence 32(3), 569–575 (2010)
33. Refaeilzadeh, P., Tang, L., Liu, H.: Cross-Validation, pp. 1–7. Springer New York, New York, NY (2016)
34. Gareth, J., Daniela, W., Trevor, H., Robert, T.: An introduction to statistical learning: with applications in R. Spinger (2013)